Eur. Phys. J. Special Topics **227**, 1173–1183 (2018)

https://doi.org/10.1140/epjst/e2018-800035-y

THE EUROPEAN PHYSICAL JOURNAL SPECIAL TOPICS

Regular Article

Mechanism of solitary state appearance in an ensemble of nonlocally coupled Lozi maps

Nadezhda Semenova[a], Tatyana Vadivasova, and Vadim Anishchenko

Saratov State University, 83 Astrakhanskaya street, Saratov 410012, Russia

Received 30 March 2018 / Received in final form 6 June 2018
Published online 12 December 2018

Abstract. We study the peculiarities of the solitary state appearance in the ensemble of nonlocally coupled chaotic maps. We show that the nonlocal coupling and features of the partial elements lead to the emergence of multistability in the system. The existence of solitary state is caused by the formation of two attracting sets with different basins of attraction. Their evolution is analyzed depending on the coupling parameters.

1 Introduction

One of inexhaustible areas of research is connected with nonlinear ensembles with a large number of elements and different network topologies, which give rise to various types of spatio-temporal dynamics. Thus, besides widely considered chimera states (see e.g., Refs. [1–12]), ensembles with nonlocal coupling can demonstrate another spatio-temporal structure, which is called "solitary state" [7–9,11,13–21]. In contrast to chimera state (which consists of spatially divided clusters of coherent and incoherent behaviour), the solitary state regime is characterized by a coherent behaviour of the whole system, except several elements. These elements do not form a cluster and for this reason these oscillators are called solitary ones.

Solitary states can be observed in ensembles with different topologies: global [13,14,21], nonlocal [7–9] and for some cases of local coupling [19]. Moreover, solitary states can coexist with chimera states and can be an intermediate regime leading to chimera emergence [7]. There is a class of partial elements for which the chimera state can be observed in ensembles with nonlocal coupling and the solitary state is not [8]. This class includes chaotic maps and chaotic time-continuous oscillators which are characterized by the transition to chaos via period-doubling bifurcations (Feugenbaum scenario). The transition from spatial coherence to incoherence in such ensembles occurs through chimera states. Peculiarities of their formation and their characteristics have been described in a number of works (see e.g., Refs. [3,8,9,22,23]). Some of them [8,9] show that the type of a chaotic attractor impacts on the appearance of different spatial structures. For example, if we consider a ring of nonlocally coupled Hénon maps (they have a nonhyperbolic chaotic attractor) this system can demonstrate chimera states. But if we replace Hénon maps with Lozi maps, which

[a] e-mail: nadya.i.semenova@gmail.com

exhibit quasihyperbolic attractors, such a system would not show chimera states and the transition to spatial incoherence would occur through solitary states [8,9].

Therefore, the question arises: "What is the bifurcation mechanism of solitary state formation in an ensemble of elements such as the Lozi map?" The present paper is dedicated to the analysis of the solitary state formation in ensemble of nonlocally coupled Lozi maps.

One of the possible mechanisms of solitary state emergence has been described in [19] for an ensemble of phase oscillators with inertia. It has been shown that solitary states arise in a homoclinic bifurcation of a saddle-type synchronized state and die eventually in a crisis bifurcation after essential variation of the parameters. Another one mechanism has been shown in [24], where the solitary state has been found in a chain of locally coupled bistable units with two stable equilibrium states. The number of steady inhomogeneous states (among them there are solitary ones) decreases with increasing the coupling strength through cascade of saddle-node bifurcations. Similar states have been observed for amplitudes and/or phases of oscillators in the ring of self-sustained nonisochronous oscillators with diffusive coupling [25]. For the both models [24,25], the appearance of solitary states is connected with bistability of partial elements.

It reveals that there are several mechanisms of solitary state emergence, and not all of them are studied. The bifurcation mechanisms and their appearance depends on the type of partial elements and the network topologies. The existence of solitary state can be explained by the bistability or multistability of the network elements. However, the multistability or bistability of one isolated partial element is not a necessary condition. Solitary states appear in the ensemble of the nonlocally coupled Lozi maps, which have only one attracting set. In the present paper we investigate an ensemble of nonlocally coupled Lozi maps and analyse in detail the dynamics of partial elements, which leads to the appearance of solitary states. We show that the nonlocal coupling can give rise to bistability in the ensemble, and this is one of the reasons of the emergence of solitary states.

2 System under study

Let us consider the ensemble of coupled maps:

$$\begin{aligned} x_i^{t+1} &= f_x(x_i^t, y_i^t) + \tfrac{\sigma}{2P} \sum_{i-P}^{i+P} [f_x(x_j^t, y_j^t) - f_x(x_i^t, y_i^t)], \\ y_i^{t+1} &= f_y(x_i^t, y_i^t), \qquad i = 1, 2, \ldots N. \end{aligned} \tag{1}$$

Here, $f_x(x_i^t, y_i^t)$ and $f_y(x_i^t, y_i^t)$ are the functions defined by the right sides of the two-dimensional Lozi map, x_i, y_i are the state variables, t is the discrete time and N is the number of elements in the ensemble. The nonlocal coupling is characterized by the coupling strength σ, the number of neighbours $2P$ (P neighbours on the either side of the ith element), and the coupling range $r = P/N$. For simplification we add the coupling only to the first equation (1). It is not essential for our investigations.

It has been shown in [8,9] that the ensemble dynamics depend on individual elements. In the present work we are focused on the system (1) with Lozi maps:

$$x^{t+1} = f_x(x^t, y^t) = 1 - \alpha|x^t| + y^t, \qquad y^{t+1} = f_y(x^t, y^t) = \beta x^t. \tag{2}$$

In this paper, we fix the parameters $\alpha = 1.4$, $\beta = 0.3$, $r = 0.2$ ($P = rN = 200$ when $N = 1000$) and change the coupling strength σ to obtain the transition from coherence to incoherence through the solitary states. These states have already been

found in works [8,9], however, no explanation has been given there. In the case of considered parameters α and β, the attractor of one Lozi map consists of two parts (gray points in Fig. 1c) and Lozi map demonstrates chaotic regime.

3 Numerical analysis of formation and evolution of solitary states in the ensemble of Lozi maps

This section is dedicated to transition from spatial coherence to incoherence via solitary states. First of all let us consider the case of spatial coherence (Fig. 1). It can be observed in a wide range of coupling parameters [8,9]. The regime of spatial coherence is characterised by a smooth instantaneous spatial profile. It means that $|x_i - x_{i+1}| < \delta$, $\delta \ll 1$ for neighbouring oscillators. Figure 1a illustrates the instantaneous spatial coherence at time $t = 10000$ for the coupling strength $\sigma = 0.27$. This figure has been obtained in the following manner. We choose 20 different sets of initial conditions distributed in the intervals $x_i^0 \in [-0.5; 0.5]$ and $y_i^0 \in [-0.6; 0.6]$. Figure 1a shows the most typical spatial profile demonstrated by the system (1) for $\sigma = 0.27$.

To show the main possible spatial profiles which the system demonstrates at different time moments, one can depict last 50 instantaneous profiles in one figure. Corresponding spatio-temporal profiles [23] are shown in Figure 1b. All spatial profiles are distributed near four curves (1,2,3,4 in Fig. 1c), but the regime is chaotic and is characterized by positive Lyapunov exponent.[1] The switching order of spatial profiles is the following 1,2,3,4,1,2,3... (see Fig. 1c). The same character of switching takes place for other regimes contained in this section.

To illustrate the difference between obtained regime and the dynamics of one Lozi map, we consider the projections of the spatio-temporal profiles (x_i^t, y_i^t) on the phase plane (x, y) of one Lozi map. Figure 1c shows the set of nonlocally coupled Lozi maps (black points) and the set demonstrated by one uncoupled isolated map (2) for the same values of system parameters (gray points). In the case of spatial coherence regime these two sets are almost identical (Fig. 1c).

The distinctive feature of the ensemble (1) of Lozi maps is that all points of the instantaneous spatial profile belong to one band of the double-band attractor. However, it does not occur in the ensemble (1) of Hénon maps (see Refs. [8,9]). Thus, we can assume that this distinction is caused by different transitions to chaos in the Hénon and Lozi maps, as it has been mentioned in Section 1.

The preparation of basins of attraction for the whole system is a very difficult problem due to imaging of $2N$ basins on the phase plane. For this reason we prepare the basin of attraction for *only one oscillator* from the stable regime. The basin of attraction for the kth oscillator can be computed as follows. We use the spatial profile shown in Figure 1a as initial conditions. Then we change the initial conditions of the kth oscillator in the intervals $x_k^0 \in [-1.5; 2]$, $y_k^0 \in [-1; 1.5]$ and make 5×10^4 iterations of the system (1) to calculate the basins of attraction for different sets. In the case of coherence regime (Fig. 1, $\sigma = 0.27$) all initial conditions of kth oscillator lead to the spatial profile shown in Figure 1. It corresponds to the left band of two-band attractor depicted in Figures 1c and 1d. No other sets have been found for this case.

Now let us decrease the coupling strength σ to obtain a solitary state regime.

When $\sigma = 0.226$, the first solitary oscillator $i = 702$ appears in the ensemble (Fig. 2a). The other oscillators stay in the coherence regime (compare Figs. 1a and 2a). Figure 2 shows the instantaneous profile (panel a), spatio-temporal profile

[1] The network (1) is considered as a dynamical system with the dimension $2N$ ($N = 1000$) and $\lambda_{\max}$ is estimated by using the standard Benettins algorithm[26]. Our calculations have indicated that the regime of spatial coherence is characterised by positive exponent. The specific value depends on the initial conditions and averaging interval.

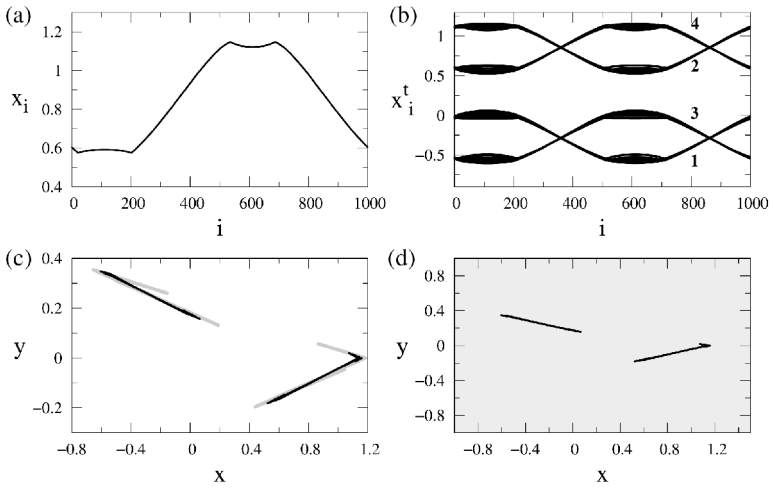

Fig. 1. Spatial coherence in the ensemble (1) of Lozi maps for $\sigma = 0.27$. Top panels illustrate the instantaneous snapshot at the time $t = 10,000$ (a) and the last 50 instantaneous spatial profiles x_i^t (b). Panel (c) depicts the projections of the spatio-temporal profiles for the ensemble (1) (black dots) on the phase plane (x, y) of one isolated Lozi map (2), and the gray points correspond to the attractor of this one map. The projections of this ensemble set and its basin of attraction on the same phase plane (x, y) are shown in panel (d) for the oscillator $k = 600$. Other parameters: $\alpha = 1.4$, $\beta = 0.3$, $r = 0.2$.

(panel b), projection of ensemble dynamics to the phase plane of one Lozi map (panel c) and corresponding basins of attraction (panel d). For better understanding we will call the oscillators which belong to the smooth spatial profile as typical oscillators, and the other elements as solitary oscillators. The corresponding sets on the phase plane (x, y) are solitary and typical, respectively. Now there are two sets on the phase plane (x, y) (Fig. 2c): black points correspond to typical set (oscillators from the smooth spatial profile) and red points agree with solitary one.

Figure 2c shows that both sets consists of two parts. This effect is caused by discrete dynamics of the considered ensemble (1). At even time moment the solitary oscillator belong to the left part of the red set (Fig. 2c), and in the next iteration (odd time) this oscillator is located in the right part. The typical oscillators from the smooth profile demonstrate similar dynamics but for the black set of Figure 2c. The appearance of two different attracting sets in one system indicates the emergence of bistability. It means that each oscillator can fall into typical or solitary set depending on the initial conditions. The bistability of the ensemble elements can be confirmed by basins of attraction for two different sets. The procedure of their preparation is the same as it was for Figure 2c with the exception of initial conditions coinciding with the spatial profile of Figure 2a. The basins of attraction have been obtained for the oscillator $k = 702$ which is solitary in the considered regime. Figure 2d shows that one can obtain the oscillator $k = 702$ in the typical or the solitary set. Their basins of attraction are shown by light gray and gray colors in Figure 2d, respectively.

The solitary set has the basin of attraction in the form of V-letter. This domain of non-zero measure is much smaller than another basin. The same basins can be obtained for the other oscillators. Nevertheless, the basin is rather narrow. Therefore, the solitary oscillator is only one for random initial conditions.

One more distinguishing feature of the solitary state is a phase shift between realizations of typical or solitary oscillators and the dynamics of the corresponding

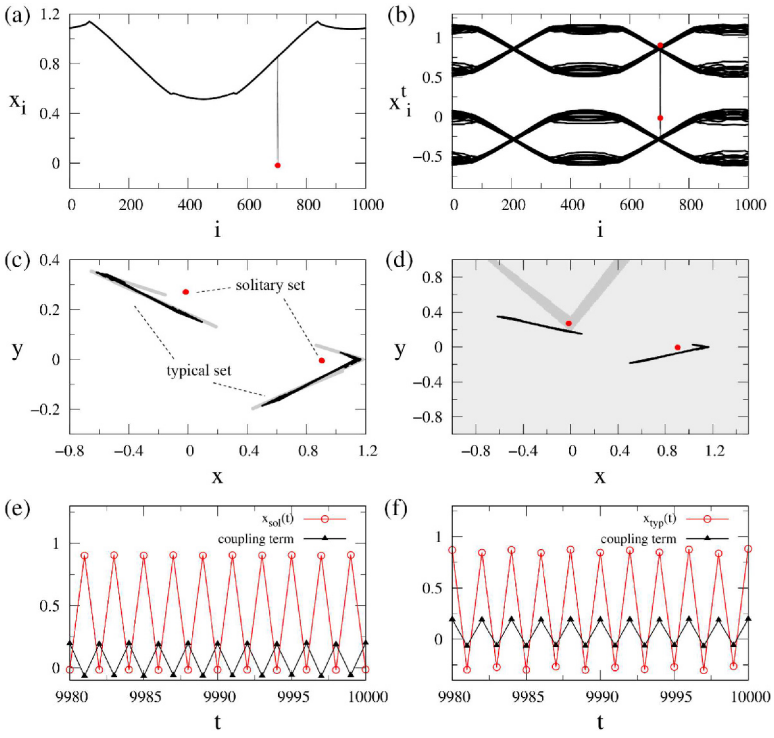

Fig. 2. Solitary state in the ensemble (1) of Lozi maps for $\sigma = 0.226$. Top panels illustrate the instantaneous snapshot at $t = 10,000$ (a) and the last 50 instantaneous spatial profiles x_i^t (b). Panel (c) depicts the projections of solitary and typical sets of the ensemble (1) on the phase plane of one isolated Lozi map (red and black points, respectively); the attracting set for one Lozi map (2) is shown by gray points. The projections of these ensemble sets (1) and their basins of attraction are shown in panel (d) for the oscillator $k = 702$. The light gray area corresponds to the basin of attraction for the typical set; the gray region is the same but for the solitary set. Panels (e) and (f) show the realizations of the system (1) for solitary oscillator ($i = 702$ in (e)) and typical oscillator ($i = 701$ in (f)) and the corresponding coupling terms $\frac{\sigma}{2P} \times \sum_{j=i-P}^{i+P} f(x_j^t, y_j^t), \quad j \neq i.$

coupling terms, i.e. impact of other coupled oscillators on each ith partial element. Equation (1) can be rewritten in the form:

$$\begin{aligned} x_i^{t+1} &= (1-\sigma) f_x(x_i^t, y_i^t) + \tfrac{\sigma}{2P} \sum_{j=i-P}^{i+P} f_x(x_j^t, y_j^t), \qquad j \neq i, \\ y_i^{t+1} &= f_y(x_i^t, y_i^t). \end{aligned} \tag{3}$$

This form of equation (1) shows the coupling term $\frac{\sigma}{2P} \sum_{j=i-P}^{i+P} f_x(x_j^t, y_j^t), \; j \neq i$ with a full picture of the impact of all coupled oscillators on the ith element. As Figures 2e and 2f show, the typical oscillator is in-phase with the coupling term and the solitary oscillator is anti-phase. This effect will be more fully described and explained in Section 4.

When decreasing of the coupling strength σ, the number of solitary oscillators increases (Figs. 3a and 3b). They start influencing on the dynamics of the whole

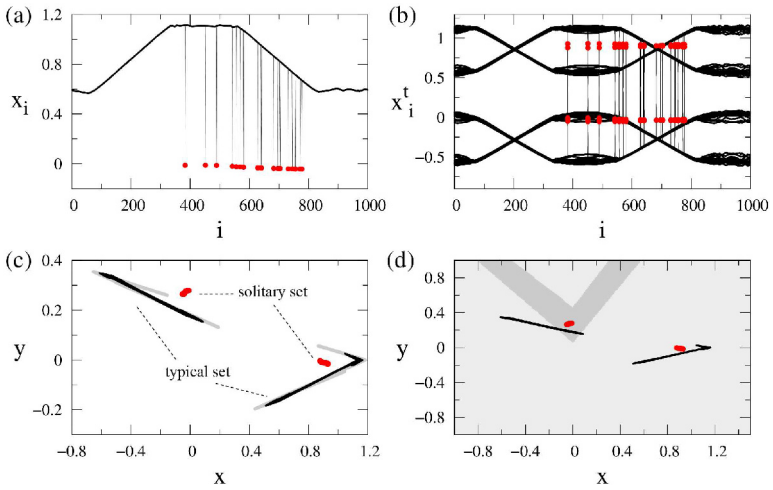

Fig. 3. Solitary state regime in the ensemble (1) of Lozi maps for $\sigma = 0.22$. Top panels show the instantaneous snapshot at $t = 10000$ (a) and the last 50 instantaneous spatial profiles x_i^t (b). Panel (c) depicts the projections of solitary and typical sets of the ensemble (1) on the phase plane of one isolated Lozi map (red and black points respectively); the attracting set for one Lozi map (2) is shown by gray points. The projections of these ensemble sets (1) and their basins of attraction are shown in panel (d) for the oscillator $k = 580$. The light gray area corresponds to the basin of attraction for the typical set; the gray region is the same but for the solitary set. Other parameters: $\alpha = 1.4$, $\beta = 0.3$, $r = 0.2$.

ensemble. For this reason, the solitary set involves new points and becomes more blurred (Fig. 3). The recorded growth leads to an enlargement of the corresponding basin of attraction (Fig. 3). This finding explains a growing number of solitary oscillators obtained from random initial conditions.

With further decreasing of the coupling strength σ, the number of solitary oscillators continues growing up, and their basin of attraction also enlarges. In this case the basin prepared for only one oscillator (like in Fig. 3d) depends on the choice of an ensemble element. This is caused by a random distribution of solitary elements in the ensemble. In some cases the basins demonstrate a fractal structure (like in Fig. 4d).

Finally, the number of "solitary" oscillators sharp increases. The ensemble demonstrates the spatial incoherence. And both sets (black and red sets in Fig. 4) have four parts and approach each other. This is the end of transition to chaotic spatial incoherence.

In such a way, Figures 2–4 depict that the decrease of the coupling strength leads to the increase of the solitary oscillators number, accompanied by the enlargement of their basins of attraction. The growing number of solitary oscillators is caused by the fact that their initial conditions falls within the increasing basin of attraction. However, using specially prepared initial conditions one can artificially increase the solitary oscillators number. To illustrate this effect we use the system in the stable regime shown in Figure 3a for $\sigma = 0.22$, choose 10 (Fig. 5a), 200 (Fig. 5b), and 400 (Fig. 5c) random oscillators and specify the same initial conditions from the basin of attraction for solitary oscillators for these elements. Figure 5 shows how the basins of attraction change (see Figs. 5a–5c). Thus, one can enlarge their basin of attraction by increasing the number of solitary oscillators. It means that the principle "the wider the basin, the larger number of solitary oscillators" works in both sides.

Thus, each kth element can become solitary if one artificially set its initial conditions in the basin of attraction for the solitary oscillators. Moreover, using specially

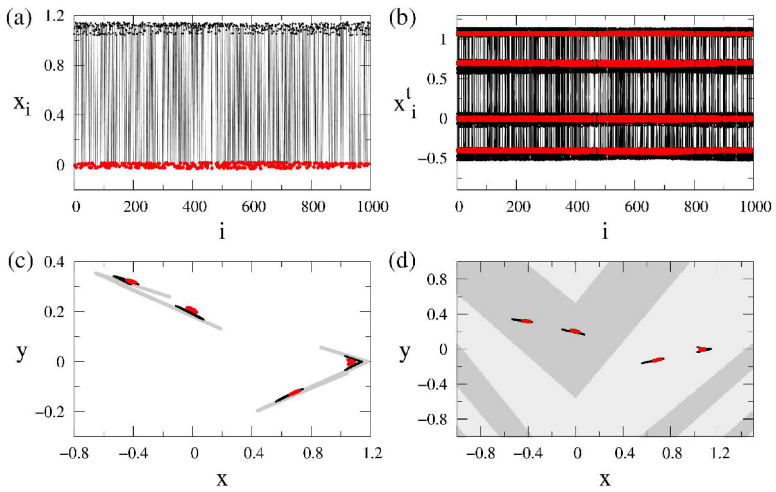

Fig. 4. Spatial incoherence in the ensemble (1) of Lozi maps (2) for $\sigma = 0.1$. Top panels reflect the instantaneous snapshot at $t = 10000$ (a) and the last 50 instantaneous spatial profiles x_i^t (b). Panel (c) shows the projections of the attracting sets for the lower oscillators (red points) and the upper oscillators (black dots) of the ensemble (1) in the phase plane (x, y) of one isolated Lozi map; the attracting set for one Lozi map (2) is shown by gray points. The projections of these ensemble sets (1) and their basins of attraction are plotted in panel (d) for the oscillator $k = 350$. The light gray area corresponds to the basin of attraction for the upper oscillators; the gray region is the same but for the lower oscillators. Other parameters: $\alpha = 1.4$, $\beta = 0.3$, and $r = 0.2$.

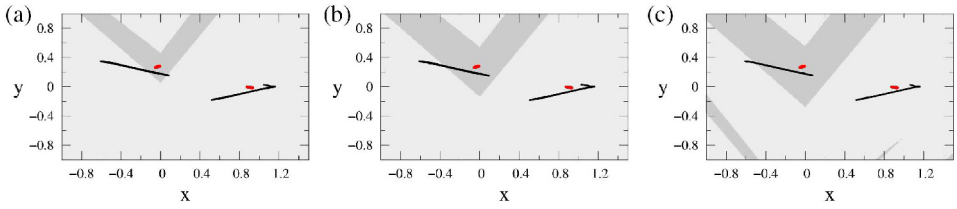

Fig. 5. Projections of the basins of attraction on the phase plane of one isolated Lozi map. The figure has been prepared choosing the initial conditions for a group of oscillators in the solitary set. The numbers of oscillators in the group are 10 (a); 200 (b); 400 (c). Parameters: $\alpha = 1.4$, $\beta = 0.3$, $\sigma = 0.22$, and $r = 0.2$.

prepared initial conditions for a group of oscillators one can create a cluster of oscillators which demonstrate the same dynamics as one solitary oscillator (Fig. 6). For that we choose the parameter $\sigma = 0.226$ corresponding to solitary state with only one solitary oscillator (Fig. 2a) and put the oscillators 300–500 to the basin of attraction for the solitary oscillators. All the parameters are the same for Figures 2 and 6. This effect confirms the existence of the second attractor and the fact that solitary state is caused by the multistability of individual elements in the ensemble (1).

4 Modelling the individual element dynamics in the ensemble (1) using a nonautonomous map

Let us consider a single element (node) of the ensemble (1) which is under the action of the neighbouring oscillators. We choose the oscillator $i = k$ and denote $x_k^t = x^t$,

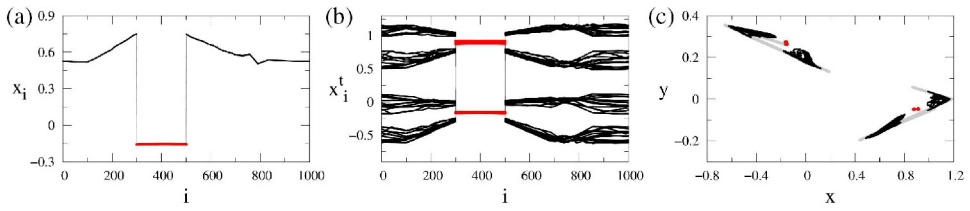

Fig. 6. Specially prepared cluster of oscillators in the solitary set. Panel (a) corresponds to the instantaneous snapshot at $t = 10,000$, panel (b) depicts the last 50 instantaneous spatial profiles x_i^t, and the panel (c) illustrates the projections of the typical (black) and the solitary (red) sets in the ensemble (1) of Lozi maps. Parameters: $\alpha = 1.4$, $\beta = 0.3$, $\sigma = 0.226$, and $r = 0.2$.

$y_k^t = y^t$. This enables us to rewrite the equation for the kth oscillator in the following form:

$$x^{t+1} = (1-\sigma) f_x(x^t, y^t) + F^t, \qquad y^{t+1} = f_y(x^t, y^t), \tag{4}$$

where $F^t = \frac{\sigma}{2P} \times \sum_{j=i-P}^{j=i+P} f(x_j^t, y_j^t) = \frac{\sigma}{2P} \times \sum_{j=i-P}^{j=i+P} (1 - \alpha|x_j^t| + y_j^t), \quad j \neq i.$

Equation (4) indicates that the coefficient σ affects the effective parameters of individual elements. In fact, if the term F^t is discarded, equation (4) can be transformed to the form (1) by letting $x = (1-\sigma)X$, $y = (1-\sigma)Y$:

$$X^{t+1} = 1 - \alpha_{\text{eff}}|X^t| + X^t, \qquad Y^{t+1} = \beta_{\text{eff}} X^t,$$

where $\alpha_{\text{eff}} = (1-\sigma)\alpha$ and $\beta_{\text{eff}} = (1-\sigma)\beta$ are the effective values of parameters.

If the coupling radius is too large, then F^t can be regarded as a mean field showing an averaging impact of neighbours on the considered element. The impact of the kth oscillator on the dynamics of the other elements in the ensemble may be ignored in the first approximation. Let us consider the case when all neighbouring oscillators are in the typical regime. It means that their instantaneous states belong to one part of the double-band attractor which is demonstrated by the autonomous map (2) with the parameters α and β. It allows us to replace F^t by a certain value x^* averaged over all x from the corresponding part of the attractor.

We now explore the system (4) for the Lozi map with parameters $\alpha = 1.4$, $\beta = 0.3$, and $\sigma = 0.226$. The ensemble (1) of Lozi maps with these parameters demonstrates the regime with only one solitary oscillator (Fig. 2). Figure 7a shows the attractor of the map (4) without the external force ($F^t = 0$) (black X-points) and the attractor of the Lozi map (2) with the effective values of parameters (light gray circles). They do not coincide because of the multiplier $(1-\sigma)$ in the first equation (4). The chosen value σ corresponds to the period-2 dynamics in the autonomous system (2). Now we add the term F^t to modulate the influence of neighbours in the ensemble. We are focused on the regime of typical state for all neighbouring oscillators. It allows us to replace their impact by averaged values of variables on one part of the Lozi attractor. Taking into account the period-4 dynamics of the typical state (see Fig. 2b) we consider every 4 value of x^t-realizations of the Lozi map (2) and then we obtain the time-mean value.

For the most part of initial conditions one can obtain the typical set shown by blue points in Figure 7a. However, some initial conditions lead to another set (red points in Fig. 7a). This set is almost the same as the set demonstrated by a single Lozi map (2) with the effective parameters α_{eff} and β_{eff}. But in the case of the system (4) with the external force, this set consists of a large number of closely spaced points.

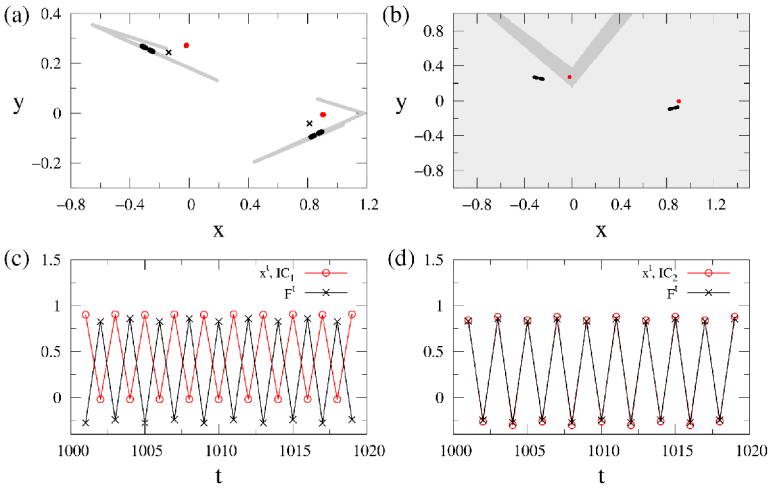

Fig. 7. Simulation results for an individual element in the ensemble (1) using the system (4). The panel (a) shows the sets which can be observed in this system: light gray circles represent the attractor of the Lozi map (2) with $\alpha = 1.4$, $\beta = 0.3$; x-points correspond to the autonomous system (4) ($F^t = 0$); red and black points indicate coexisting sets which can be observed for different initial conditions with $\sigma = 0.226$ and $F^t \neq 0$. Their basins of attraction are shown in (b). The light gray region in the panel (b) conforms to the black set and the gray region corresponds to the red set. Panels (c) and (d) depict the external force F^t and realizations of the system (4) in the typical regime (d) [black points in panel (a)] and in the "solitary" one (c) [red points in the panel (a)].

The basins of attraction for these two coexisting sets are shown in Figure 7b for the left part of the blue set and the right part of the red set. It can be seen that the red set has a V-form of the basin. The same form has been obtained for solitary states (Fig. 2d) in the ensemble (1).

What is the mechanism of occurrence of two stable regimes in the nonautonomous oscillator (4)? To answer this question, it is enough to compare their realizations with the external force wave form. The corresponding curves are shown in Figures 7c and 7d. It is obvious that both regimes in the system (4) represent in-phase and anti-phase synchronizations of self-sustained oscillations (periodic or almost periodic) by the external force, which is also periodic. In contrast to the in-phase regime, the anti-phase mode has a narrow basin of attraction (IC_1). The same results have been obtained for the ensemble (1) (see Figs. 2e and 2f). The oscillations of the solitary element $k = 702$ are anti-phase with respect to other oscillators from the typical regime and the coupling term $\frac{\sigma}{2P} \times \sum_{j=i-P}^{j=i+P} f(x_j^t, y_j^t)$, $j \neq i$. The typical oscillators represent in-phase synchronization (Fig. 2f).

Thus, the model (4) enables us to understand the mechanism of appearance of solitary states in the ensemble of Lozi maps. The coexistence of two sets and their location above and below the attractor of the autonomous map (2) harmonize with the results for the ensemble (1) (compare Figs. 2 and 7). On the other hand, there is no quantitative correspondence between these two systems. It is caused by the neglecting impact of the considered oscillator on the external force. For the limiting cases of large and small values of the coupling strength, the model (4) looses its correlation with the ensemble dynamics. The system (4) does not take into account synchronization between elements for strong σ and the impact of the other solitary states for weak coupling σ.

The mechanism described above is realized if the following conditions are met: (1) the force F^t has to be periodic or has to possess a periodic component; (2) the periodic force must lead to coexisting regimes of in-phase and anti-phase synchronization obtained for different initial conditions. In this case oscillations have to exhibit also a periodic component; (3) the induced regime of anti-phase synchronization should have a narrow basin of attraction. It leads to a small number of initial conditions which provides this set. All these conditions are fulfilled in the ensemble (1) of Lozi maps in contrast to a similar ensemble of Hénon maps.

5 Conclusions

The numerical results presented above describe one of the possible mechanisms for solitary state formation in an ensemble of nonlocally coupled oscillators. As we have anticipated, it differs from the mechanism proposed in [19]. It is caused by a principally different dynamics of individual elements. We have studied the ensemble of Lozi maps which demonstrate a quasihyperbolic chaotic attractor.

It is shown that the ensemble of nonlocally coupled Lozi maps demonstrates the solitary state for specific values of coupling parameters. The coupling changes the properties of partial elements, and leads to the bistability, though the Lozi map do not have this property in the uncoupled form. The emergence of solitary states is accompanied by the arising of the second attracting set for the ensemble element. In the present work, we investigate its basin of attraction and show that this basin increases with decreasing of the coupling strength. For this reason, the number of solitary oscillators grow too.

One can artificially increase the number of solitary oscillators and even make the cluster of elements which demonstrate the dynamics similar to one solitary oscillator. It can be done using specially prepared initial conditions and setting the initial conditions of chosen oscillators in the basin of attraction for solitary oscillators.

We have shown that the changes in the dynamics of an individual oscillator are caused by an almost periodic external influence from the neighbours. This means that all neighbours belong to the same part of the Lozi attractor.

It has been shown that in a wide range of the coupling parameter, the partial elements in the ensemble demonstrates dynamics with a clearly produced periodic component. As a result, one can obtain either in-phase or anti-phase synchronization for different initial conditions. The last one regime of the ensemble element has a narrow basin of attraction and corresponds to the solitary oscillators. The other oscillators, which are in-phase synchronized, are typical ones, since their initial conditions does not belong to the basin of attraction for solitary oscillators.

We suppose that there are different ways of the solitary state appearance. This paper describes the mechanism for the ensemble of chaotic Lozi maps. However, the peculiarities of the mechanism may depend on a type of individual elements and their interplay.

This work was supported by the Russian Ministry of Education and Science (Project Code 3.8616.2017/8.9) and by the Russian Science Foundation (Grant No. 16-12-10175).

References

1. Y. Kuramoto, D. Battogtokh, Nonlinear Phenomena Complex Syst. **5**, 380 (2002)
2. D.M. Abrams, S.H. Strogatz, Phys. Rev. Lett. **93**, 174102 (2004)
3. I. Omelchenko, Y. Maistrenko, P. Hövel, E. Schöll, Phys. Rev. Lett. **106**, 234102 (2011)

4. I. Omelchenko, O.E. Omel'chenko, P. Hövel, E. Schöll, Phys. Rev. Lett. **110**, 224101 (2013)
5. A. Zakharova, M. Kapeller, E. Schöll, Phys. Rev. Lett. **112**, 154101 (2014)
6. M.J. Panaggio, D.M. Abrams, Nonlinearity **28**, R67 (2015)
7. P. Jaros, Y. Maistrenko, T. Kapitaniak, Phys. Rev. E **91**, 022907 (2015)
8. N. Semenova, A. Zakharova, E. Schöll, V.S. Anishchenko, Europhys. Lett. **112**, 40002 (2015)
9. N. Semenova, E. Rybalova, G. Strelkova, V.S. Anishchenko, Regul. Chaotic Dyn. **22**, 148 (2017)
10. Q. Dai, M. Zhang, H. Cheng, H. Li, F. Xie, J. Yang, Nonlinear Dyn. **91**, 1723 (2018)
11. R. Gopal, V. Chandrasekar, D. Senthilkumar, A. Venkatesan, M. Lakshmanan, Commun. Nonlinear Sci. Numer. Simul. **59**, 30 (2018)
12. S. Ghosh, A. Zakharova, S. Jalan, Chaos Solitons Fractals **106**, 56 (2018)
13. Y. Maistrenko, B. Penkovsky, M. Rosenblum, Phys. Rev. E **89**, 060901 (2014)
14. J. Hizanidis, N. Lazarides, G.P. Tsironis, Phys. Rev. E **94**, 032219 (2016)
15. J. Hizanidis, N. Lazarides, G. Neofotistos, G. Tsironis, Eur. Phys. J. Special Topics **225**, 1231 (2016)
16. V. Semenov, A. Zakharova, Y. Maistrenko, E. Schöll, EPL **115**, 10005 (2016)
17. K. Premalatha, V.K. Chandrasekar, M. Senthilvelan, M. Lakshmanan, Phys. Rev. E **94**, 012311 (2016)
18. K. Premalatha, V.K. Chandrasekar, M. Senthilvelan, M. Lakshmanan, Phys. Rev. E **95**, 022208 (2017)
19. P. Jaros, S. Brezetsky, R. Levchenko, D. Dudkowski, T. Kapitaniak, Y. Maistrenko, Chaos **28**, 011103 (2018)
20. K. Sathiyadevi, V.K. Chandrasekar, D.V. Senthilkumar, M. Lakshmanan, Phys. Rev. E **97**, 032207 (2018)
21. I.A. Shepelev, T.E. Vadivasova, Rus. J. Nonlinear Dyn. **13**, 317 (2017)
22. I. Omelchenko, B. Riemenschneider, P. Hövel, Y. Maistrenko, E. Schöll, Phys. Rev. E **85**, 026212 (2012)
23. S. Bogomolov, A. Slepnev, G. Strelkova, E. Schöll, V.S. Anishchenko, Commun. Nonlinear Sci. Numer. Simul. **43**, 25 (2017)
24. J.P. Keener, SIAM J. Appl. Math. **47**, 556 (1987)
25. V.I. Nekorkin, V.A. Makarov, M.G. Velarde, Phys. Rev. E **58**, 5742 (1998)
26. G. Benettin, L. Galgani, J. Strelcyn, Phys. Rev. A **14**, 2338 (1976)